Exploding High Frequency Oscillations in an AC Driven Negative-Differential Resistor

Myeong-gi Jo,[1, a)] Subin Kim,[1, b)] Jeong Min Lee,[1, c)] and Eugene Park[1, d)]
Department of Physics and Astronomy, Seoul National University

(Dated: 25 January 2024)

A nonlinear negative differential resistor designed using an inverted operational amplifier has shown periodic high-frequency oscillations embedded in a normal linear response. These 'exploding' high-frequency oscillations occur when the negative resistor voltage increases and escapes a single stable branch of the $I-V$ curve of the negative resistor. Based on this analysis, the threshold driving frequency for such oscillations to appear has been analytically derived. A model using properties of the self-sustaining dynamic hysteresis for the high-frequency oscillation explosion around the $I-V$ curve has been constructed, accurately producing the experimental results. Analysis of the duration of these high-frequency oscillations shows that they only increase in integer numbers of the period. Furthermore, we have identified the dependence of the threshold driving frequency, high-frequency oscillation duration, and explosion oscillation frequency, which suggest easily tunable characteristics with possible applications for electronic oscillators with two-timescale dynamics.

I. INTRODUCTION

The study of nonlinear negative differential resistors goes beyond conventional boundaries, exploring a diverse range of physical phenomena and intricate systems. These nonlinear negative differential systems can be classified into two main types based on the $I-V$ curve: (1) a single-valued $V(I)$ function, seen in nonlinear resistors for the Chua[1,2] and the Van der Pol oscillator[3], and (2) a single-valued $I(V)$ function, such as systems used for dynamic hysteresis[4,5], and stochastic resonance[6].

From our previous work[7], we have designed a tunable negative differential resistor using an inverted Op-Amp and MOSFETs. This type of nonlinear differential negative resistor is the type of (2) explained above. This work will focus on creating dynamical hysteresis dynamics for the simple negative resistor designed, using a single inverted Op-Amp. The corresponding circuit diagram is shown in FIG. 1 (a) where the region between the two voltage ends V_{NR} denotes the voltage drop across the negative differential resistor.

The operation of the negative differential resistor is as follows. The negative differential resistor inverts the polarity in the unsaturated Op-Amp region, resulting in negative differential resistance. After saturation occurs in the Op-Amp for higher applied voltages, the excess current is 'vented', resulting in a linear positive differential resistance.

Forced oscillation persisting only on such positive differential regions results in a linear response. However, for conditions where the forced oscillation causes the voltage of the negative differential resistor to escape a positive differential resistance regime, the current is 'launched' out of the stable branch of positive differential resistance and induces a series of high-frequency oscillations. These high-frequency oscillation phenomena will be referred to as 'oscillation explosion'. To our knowledge, such oscillations arising from dynamical hysteresis in an AC driven system have not been studied. In this work, we derive an analytical expression of the explosion regime and develop a phenomenological model to explain quantitatively the observed phenomena. Furthermore, the results of each region analyzed in our work are directly applicable to developing designing schemes for electronic oscillators that require periodic two-timescale dynamics, such as electronic neuron oscillators implementing similar devices[8].

The paper is organized as follows. First, we discuss our experimental design and the oscillation explosion that we observed. Then, the theoretical formulation to explain this phenomenon with a simulation model is discussed. Next, we analyzed the oscillation explosion in detail, especially the driving frequency where the explosion occurs time duration that the explosion maintains. Finally, we concluded our analysis with the significance of our work.

II. METHODS

1. Design and Implementation of the Experiment

The circuit diagram used for experimentation is shown in FIG. 1 (a). The negative differential resistor designed is connected in series to an inductor and capacitor, driven with a sinusoidal voltage source of amplitude V_0 and frequency f_0. The current (via resistor R) and negative resistor voltage V_{NR} were measured using an Analog Discovery 2 at a sampling rate of 290kHz, which was near maximum. The components were soldered to minimize noise.

Preliminary experimentation has shown that oscillation explosion occurs when the driving frequency exceeds a certain threshold frequency. The experimental procedure is divided into finding the critical explosion frequency(f_{exp}) for a given voltage source amplitude(V_0) and sweeping the driving frequency and voltage amplitude around the explosion regime. The high-frequency oscillation dynamics were analyzed for three different inductance $L = 1, 10, 100$mH. The high-frequency oscillation dynamics such as the different os-

[a)]whaudrl4005@gmail.com
[b)]subini0213@snu.ac.kr
[c)]jmleeluck@snu.ac.kr
[d)]eupark@snu.ac.kr

cillation waveforms for the case of $L = 1$mH exceed the measurable time scale, thus only the explosion regime and high-frequency oscillation duration were analyzed.

2. Numerical Simulations

A simulation using the 4th order Runge-Kutta method was carried out to produce the dynamics of the experimentally observed results. A step size of $dt < 0.0000001$s was used, and the theoretical models the system as a driven bistable nonlinear resistor that can show hysteresis. The model also assumes that the solution jumps to a different bistable branch once the current meets the end of each branch. A detailed explanation of the modeling of the system, corresponding parameters used, and the differential equation with numerical methods are in Appendix B.

3. High–Frequency Oscillation Duration Algorithm

We evaluated high-frequency oscillation duration by checking the difference between adjacent data. We first set the threshold of difference and then searched for the difference that is above the threshold, i.e. the beginning of the explosion in chronological order. The end of the explosion was determined when the differences became smaller than the threshold for more than 30 steps. Since the frequency in the explosion regime and the non–explosion regime differs by more than one order of magnitude, this simple method will give a proper value of duration if the threshold is well given. We set the threshold as $\Delta V_{\text{th}} = 0.1$V for $L = 1$mH and 10mH and $\Delta V_{\text{th}} = 0.05$V for $L = 100$mH.

III. RESULTS

A. High Frequency Oscillation Explosion

Under various driving conditions, two different dynamical responses have been found in the system. In contrast to the normal oscillation having a frequency of the voltage source, regions in the time of high-frequency oscillations have been observed. For example, FIG. 1 (b) shows an ordinary oscillation observed of V_{NR}, where FIG. 1 (c) shows time windows of high-frequency oscillations between normal oscillations.

This oscillation phase can be further detected by Fast Fourier Transform (FFT), where a high-frequency component appears (FIG. 1) (d). The relatively broad spectrum and multiple peaks suggest that such frequency oscillations are not sinusoidal, thus arising from the nonlinear effects of the circuit.

B. Oscillation Explosion Regime

The current range of positive differential resistance region of oscillation without explosion is limited. From the limit, the

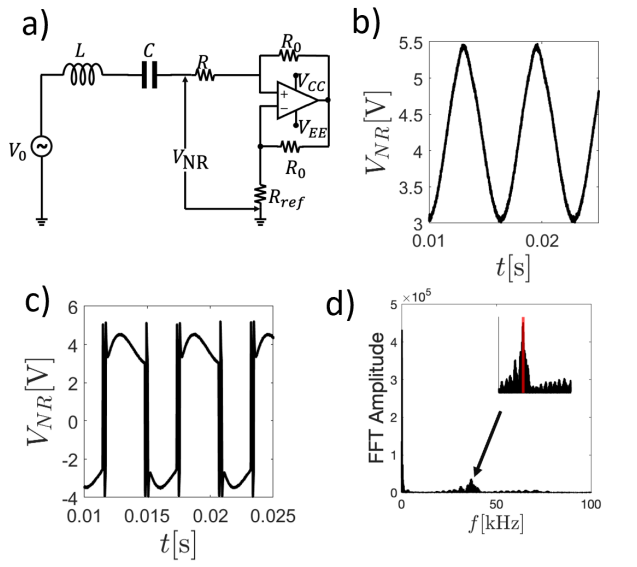

FIG. 1. a) The schematic of the circuit used, where V_{NR} denotes the nonlinear negative differential resistor voltage. $R_0 = 1\text{k}\Omega, R = 560\Omega, R_{\text{ref}} = 1120\Omega, C = 0.47\mu$F are fixed throughout the experiment. The b) normal oscillations ($f_0 = 150$Hz) and c) exploding high-frequency oscillations ($f_0 = 165$Hz) are shown for comparison. $L = 100$mH, $V_0 = 5$V was used for both cases. d) The FFT spectrum of c), shows the high-frequency oscillations (inset).

explosion threshold angular frequency is theoretically calculated as

$$\omega = I_m \frac{a}{C} \frac{1}{\sqrt{a^2 V_0^2 - I_m^2}} \tag{1}$$

Where I_m is maximum current amplitude, V_0 is driving amplitude, C is capacitance, and positive differential resistance range of negative resistance has current-voltage relation of $I = aV_R + b$.

This phenomenon can be directly observed from the $I - V$ curves under AC driving. As can be seen in FIG.1 (a), the oscillations before explosion stay on the positive differential resistance branch, while once the driving frequency exceeds f_{exp}, the system jumps out of the branch and oscillates around the two branches.

The experimentally found f_{exp} for $L = 1, 10, 100$mH for various source voltage amplitudes are compared with the analytical relation (1) (FIG. 2 (b)). From the good fit between theory and experimental results, the model and the assumption of negligible inductance to the explosion frequency can be validated. The experimental results exhibit minor deviation near the non-explosion area, which is likely to be due to the systematic error of capacitance or voltage amplitude, which is critical near the asymptote.

Furthermore according to (1), the explosion frequency is imaginary in the case $aV_0 < I_m$. Therefore the explosion frequency does not exist when the driving voltage amplitude is under a certain threshold. This threshold voltage is obtained

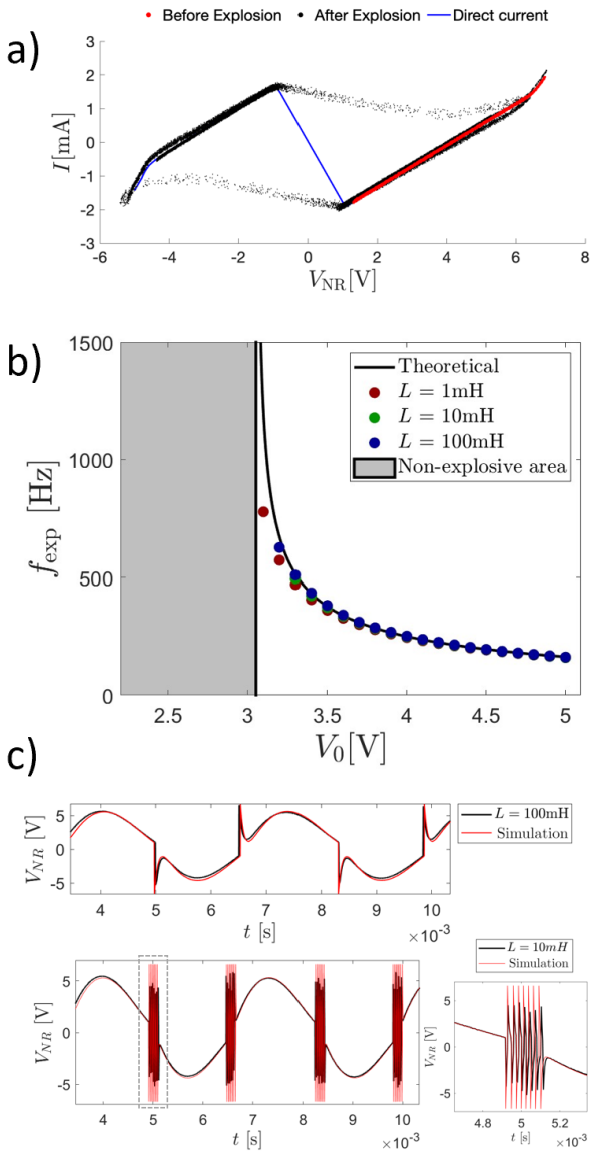

FIG. 2. a) Comparison of the $I-V$ curves for the DC voltage source, before and after the explosion of high-frequency oscillations in AC driving. $L = 100$mH, $V_0 = 5$V was used. b) The critical driving frequency(f_{exp}) as a function of V_0. The experimental values denote points where the exploding oscillations first occur, and exploding oscillations persist for $f_0 > f_{\text{exp}}$ in the experimented region. Error bars are smaller than the marker. c) The simulated (refer to simulation in Appendix. B) and experimental $V_{\text{NR}}(t)$ for $L = 10, 100$mH. The inset shows an enlarged region bounded by gray dashed lines in $L = 100$mH. The time axis was shifted to fit the experimental data.

to be about $V_{\text{th}} \approx 3.05V$.

The oscillation explosion can be also obtained with the numerical simulations from the theoretical model of the system. The simulation results match the experimental curve well, producing the dynamics of both the slow time scale linear oscillations and the fast time scale explosion oscillations. The discrepancy between the high-frequency oscillations and simulation results in the $L = 10$mH (FIG.2 (c)) is because the insufficient sampling rate could not capture the sharp peaks of each oscillation. Note that the peaks are relatively well captured experimentally for a slower $L = 100$mH system.

The peaks in the explosion oscillations occur from the exponential decay of the current in a single positive differential resistance branch, with a successive jump to the other branch, as described in Appendix B. This further explains the multi-frequency spectrum of the explosion frequencies, such repeated exponential decays produce the unique spectra. This also associates the high-frequency to have a $\sim R/L$ dependence, since the exponential decay in each spike decays at such a rate (Appendix B).

C. Oscillation Explosion Spectrum

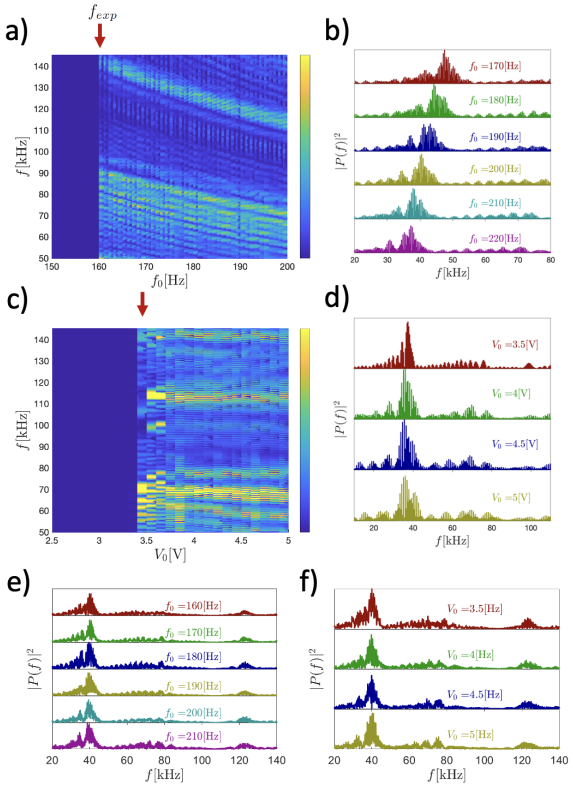

FIG. 3. a) A spectrogram for driving frequency f_0 and b) a selected group of frequencies for clarity. The explosion of high-frequency oscillations can be observed at f_{exp}, denoted by the red arrow. The high oscillation frequencies show a decrease in higher driving frequencies. c) Squared FFT amplitudes for driving voltage amplitude V_0 and d) a selected group of amplitudes for clarity. The explosion of high-frequency oscillations can be observed in the red arrow. $L = 10$mH was used.

Oscillation explosion occurs when the driving frequency f_0 and voltage amplitude V_0 are greater than some specific threshold. FIG. 3 (a), (c) show the spectrogram of V_{NR} in the vicinity of the explosion oscillation frequency, under

varying f_0 and V_0. For $f_0 \leq 160\text{Hz} = f_{\text{exp}}$ and $V_0 \leq 3.4\text{V}$ no high frequency components exist. However, after oscillation explosion, high-frequency components appear.

The squared FFT amplitudes for selected values of f_0 and V_0 are shown in FIG. 3 (b) and (d). The peak frequency of the high-frequency components shows a decrease for increasing f_0 while having no V_0 dependence.

The squared FFT amplitudes for the same selected conditions were obtained from the numerical simulations conducted(FIG. 3 (e) and (f)). Note the similar shape and the peak frequency. The spectra are independent of V_0, in line with experiments. However, simulations do not show a decrease in the peak frequency of the high-frequency components for increasing f_0. The discrepancy between the simulation and experiment may result from the non-idealistic characteristics in our devices, such as parasitic capacitance in the Op-Amp, or stem from more complex ultrafast dynamics that occur when the system jumps to another positive differential resistance branch. This, however, is out of the scope of this work and should be resolved with instruments with a higher sampling rate.

D. Duration of Explosion Oscillation

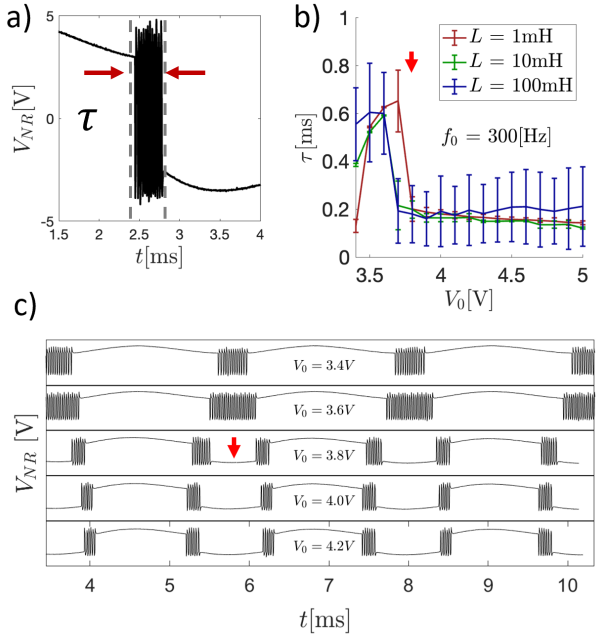

FIG. 4. a) A segment of the oscillation curve with the duration of high-frequency oscillations(τ) is denoted. b) Experimental τ by different inductance(L), for different driving voltage amplitudes(V_0). The arrow shows a sudden decrease of τ. c) A series of experimental exploding oscillations by increasing driving voltage amplitude. The red arrow denotes where the high-frequency oscillations start to split.

Our system enters and escapes the high-frequency oscillations periodically. By measuring the duration τ (FIG. 4 (a)) of the explosion oscillation stage, i.e., how long the system is under fast oscillation, interesting nonlinear relations between τ and f_0 and between τ and V_0 were observed.

The dependence of the duration of explosion oscillations(τ) with varying voltage amplitude(V_0) increases at low voltages and then decreases abruptly after a certain voltage amplitude. After the drop in τ, τ is near constant. This dependency is uniform among different inductances, with similar duration times after the abrupt decrease.

This tendency of τ can be well explained using the theoretical model constructed. For the system to jump between the two positive differential resistance branches, the driving voltage has to be sufficiently large to launch the system of the current branch. Right after a high-frequency oscillation explosion, the voltage amplitude is sufficient to launch the system of a branch, but insufficient to pertain to a stable oscillation on the other branch($V_0 = 3.4\text{V}$ in FIG. 4 (c)). Until the voltage amplitude is sufficient enough to pertain to a stable oscillation on the other branch, the time window with unstable driving voltage values increases causing τ to increase($V_0 = 3.6\text{V}$ in FIG. 4 (c)). Once the voltage amplitude is sufficient enough to pertain to a stable oscillation, the explosion oscillation splits, causing an abrupt decrease in individual τ(FIG. 4 (c), red arrow). After this split, the increase in voltage amplitude cannot cause a substantial decrease in τ.

In the $L = 100\text{mH}$ experiment, its statistical error was significantly larger than in the $L = 1, 10\text{mH}$ experiments. This is because there are fluctuations in the number of periods in the explosion regime. In the $L = 1, 10\text{mH}$ experiments, there are $O(10^1)$ periods per explosion, so the difference of one or two periods is negligible. However, in the 100mH experiment, there are $1/2 - 3/2$ periods per explosion, thus τ varies up to three times due to the fluctuation. This resulted in inevitable statistical errors despite of large number of explosion data.

For the τ dependency on driving frequency, an increase in driving frequency causes the system to pass through the explosion region faster, causing a decrease in the duration. This can be seen in the $\tau \propto \frac{1}{f_0}$ of FIG.5 (a).

However, a much more complex phenomenon is observed for higher inductance. For the $L = 10, 100\text{mH}$ experiments, clear steps are in the experimental data of values $\Delta\tau \sim 0.017\text{ms}, \Delta\tau \sim 0.1\text{ms}$, respectively. Such steps in τ stem from the high-frequency oscillations only increasing in integer values of a hysteresis loop around the $I - V$ curve. The single oscillation period depicted in red arrows of 5 (c) and (d) show the period of a single explosion oscillation to be $\sim 0.031\text{ms}$ and $\sim 0.23\text{ms}$ for $L = 10$ and 100mH, respectively.

The value of a period of high-frequency oscillation being $\sim 2\Delta\tau$ is because there are two explosion oscillation windows, each corresponding to a driving voltage increase and decrease. As seen in 5 (c) and (d), each window does not simultaneously increase by a single period. Instead, a single period is added in alternating order to each window. Note this is not observed for $L = 1\text{mH}$, since the steps in τ are insufficient in magnitude.

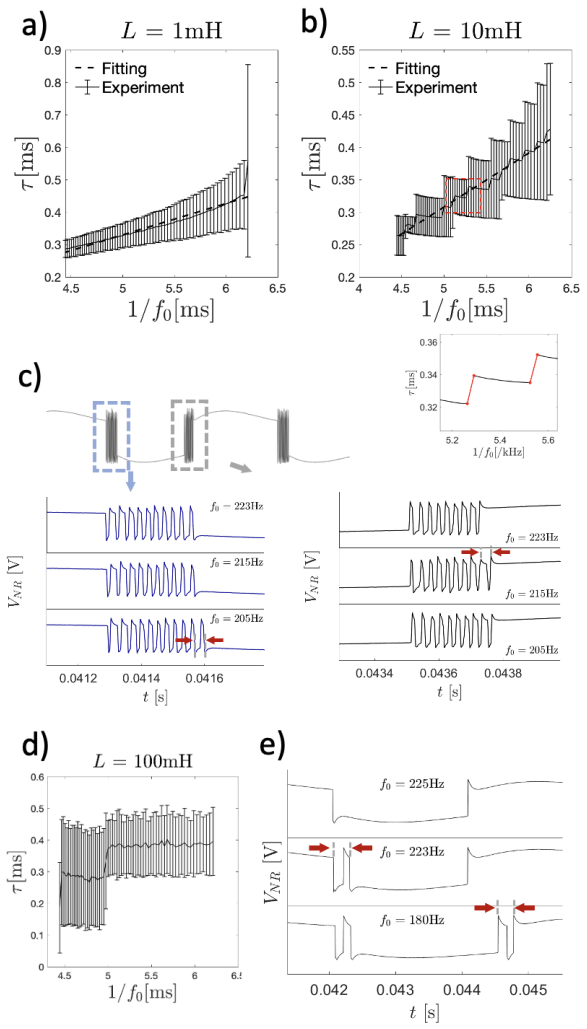

FIG. 5. a) τ of $L = 1$mH for different driving frequencies. The dashed line shows a linear fit. b) τ of $L = 10$mH for different driving frequencies. The stair-shaped average of τ is enlarged for the red-boxed region in the smaller figure below. The red lines denote the height of each step. c) Experimental high-frequency oscillations for $L = 10$mH at three different driving frequencies. The blue-boxed region corresponds to the blue curves, and the gray-boxed region corresponds to the black curves. An addition of one $I-V$ curve oscillation is shown with the red arrows. The time axis was shifted for clarity. d) τ of $L = 100$mH for different driving frequencies. e) Experimental high-frequency oscillations for $L = 10$mH at three different driving frequencies. An addition of one $I-V$ curve oscillation is shown with the red arrows. The time axis was shifted for clarity.

IV. CONCLUSION

The system we have shown exhibits a unique high-frequency oscillation, occurring in the form of dynamic hysteresis. We note that however, these oscillations exhibit frequencies of an order of magnitude higher than the conventional dynamic hysteresis[5]. Furthermore, an analytical expression for such oscillation explosion has been shown, with a good fit with experimental data. The simulations based on the $I-V$ characteristics at these high-frequency oscillations have been shown to produce the phenomena well and demonstrate the dynamics and characteristics of such high-frequency oscillations. This further implies that the high-frequency oscillation is derived from a self-driving dynamic hysteresis in the nonlinear negative differential resistor. The driving frequency dependence of the oscillation frequency has a deviation from the experiment, showing that these effects can be attributed to the ultrafast dynamics of jumps of the hysteresis. The duration of these high-frequency oscillations has been shown to increase until the splitting of the explosion oscillation window occurs and then decreases abruptly afterward. Additionally, analysis of this duration by driving frequency shows that the high-frequency oscillations increase in an integer number of cycles.

Furthermore, we note the dependence of different characteristics of the high-frequency oscillation. The explosion threshold frequency is dependent on V_0, C; the explosion oscillation frequency is dependent on $f_0, R/L$; and the high-frequency oscillation duration is dependent on V_0, f_0. This implies that given a targeted oscillation duration τ, explosion oscillation frequency, and explosion threshold frequency, the parameters of the circuit V_0, f_0, C, L can all be chosen to meet these requirements. This provides powerful tuning possibilities, and paving methods for implementing this device for electronic oscillators requiring two tunable two-timescale dynamics, such as spiking oscillators[8,9]. The simple circuit holds advantages over other circuits due to its simplicity and robustness. Previous work on tuning the negative differential resistor[7] further expands this possibility.

Despite this extensive analysis, the ultrafast dynamics of such an oscillator has not been investigated due to experimental limitation. The ultrafast dynamics of this oscillator with the implementation of spiking oscillators will be a further research topic that can fully enable the advantages of the phenomena investigated.

Appendix A: Derivation of the theoretical explosion frequency

The oscillation can be maintained without explosion if and only if the voltage difference through the negative resistor is in the positive-differential resistance region. This region has a minimum current value; which is negative, so the current has an amplitude limit, and explosion occurs when stable oscillation requires a lower current than the limit. Before the explosion, the signal has a low frequency in our experimental range, so the effect of the inductance is negligible. In this case, we can write a differential equation about capacitor charge such as

$$V_d(t) = V_R + \frac{Q}{C} \tag{A1}$$

$$V_R = \frac{I-b}{a} \tag{A2}$$

where Q is charge, I is current, V_d is driving voltage, anda, b

are coefficients of $I = aV_R + b$, positive linear region of negative resistor. Using time derivation, these are driven to

$$\dot{I} = a\dot{V}_d - \frac{a}{C}I \tag{A3}$$

$$I_0 = \frac{i\omega}{ß\omega + a/C} aV_0 \tag{A4}$$

where solving equation by $V_d = V_0 e^{i\omega t}$, $I = I_0 e^{i\omega t}$. The equation determines the amplitude of current by frequency and voltage amplitude. As we have current amplitude limit of I_m, frequency limit is

$$\omega \leq I_m \frac{a}{C} \frac{1}{\sqrt{a^2 V_0^2 - I_m^2}} \tag{A5}$$

and

$$f_{exp} = I_m \frac{a}{2\pi C} \frac{1}{\sqrt{a^2 V_0^2 - I_m^2}} \tag{A6}$$

becomes the formula of explosion frequency.

Appendix B: Runge-Kutta Simulations

The theoretical motion is based on the bisTable curves of the inverted op-amp negative resistor. Although the system can reach the negative differential resistance region, shown in previous reports, under AC driving the experimental results show the system oscillates between the two stable branches of the $V - I$ curve. Once the trajectory of escapes a certain branch, the next branch is immediately selected. The overall model is shown in FIG.6.

The theoretical explanation of the phenomena is given as the following.

1. On the stable branches, the solution follows the Kirchoff relations given by the characteristics of the branch. Thus, dynamics on the stable branches can be solved analytically and theoretically.

2. Once the solution passes the end of the branch, which the criteria is $I > I_{m1}$ (b1), $I < -I_{m3}$ (b3), there is no stable solution that extends the branch. Thus, the solution immediately jumps to the branch where a voltage V_{NR} is defined for the given current I_{NR}.

3. The current and charge of the capacitor do not change upon a jump to the different branch, since the current should act continuously and the charge cannot be discontinuous without an infinite delta-function-like change in the current.

4. The current and charge continue to satisfy the Kirchoff equations on the new branch, and the process is repeated.

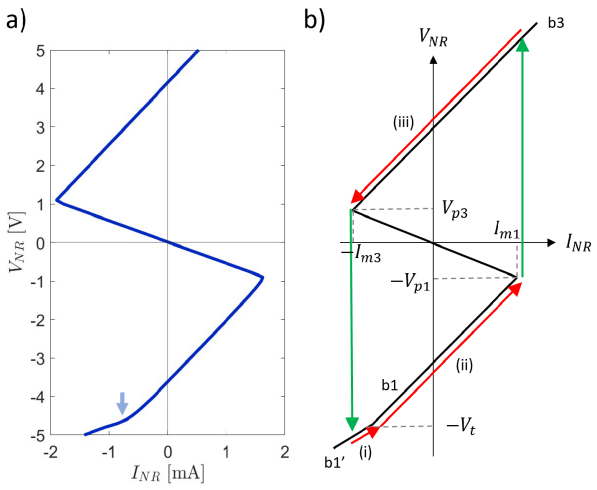

FIG. 6. a) The actual $I_{\mathrm{NR}} - V_{\mathrm{NR}}$ characteristics of the negative differential resistor used, which is obtained by measuring current flow from a given voltage source. The $I_{\mathrm{NR}} - V_{\mathrm{NR}}$ axis was exchanged for clarity in comparison. b) The simulation model. Note the branch change in a) denoted by an arrow is also included in the model. b1, b1′ denote the lower branches, b3 denotes the upper branch. Green arrows show jumps to the next stable branch, and the red arrows are regions solved for the dynamics, denoted as (i), (ii), and (iii). Parameters such as V_{p1}, V_{p3}, I_m are depicted.

TABLE I. Parameters used for the Runge-Kutta simulations and their corresponding experimental values. The mean values were used for simulation. R_i, R_{ii}, R_{iii} denote the resistance for each branch (i), (ii), (iii)

Parameter	Value
I_{m1}	1.9 ± 0.2 mA
I_{m3}	1.6 ± 0.2 mA
V_{p1}	1.1 ± 0.1 V
V_{p3}	0.9 ± 0.1 V
V_t	4.6 ± 0.1 V
R_i	547 ± 21 Ω
R_{ii}	1600 ± 4.3 Ω
R_{iii}	1620 ± 7.5 Ω
L	1mH, 10mH, 100mH[a]
C	0.47 μF
V_0	5 V

[a] Corresponding to experiment

Before any theoretical analysis, an appropriate model should be made for the negative differential resistor. Thus, the experimental values FIG.6 a) were fitted from, resulting in the following values that were used.

We note that the exploding oscillations are not sensitive to such parameters, and can be achieved with other values when the exploding criteria are met. However, a detailed modeling of the $I - V$ characteristics was required to produce the waveforms of fast oscillations experimentally observed.

For each branch, the Kirchoff equations give a 2nd order differential equation. Given the function of the branch as

$V_{\mathrm{NR}} = f_{bi}(I_{\mathrm{NR}})$, the following voltage relation can be given.

$$V_0 cos(\omega t) = V_L + V_C + V_{\mathrm{NR}} \tag{B1}$$

Plugging the appropriate values, the following equation can be obtained, where q denotes the charge in the capacitor.

$$V_0 cos(\omega t) = L\ddot{q} + q/C + f_{bi}(\dot{q}) \tag{B2}$$

$$f_{b1'}(I) = V_t + R_i \left(I - \left(I_{m1} + \frac{V_{p1} - Vt}{R_{ii}} \right) \right) \tag{B3}$$

$$f_{b1}(I) = -V_{p1} + R_{ii}(I - I_{m1}) \tag{B4}$$

$$f_{b3}(I) = -V_{p3} + R_{iii}(I - I_{m3}) \tag{B5}$$

Using the relation $I = \dot{q}$ and adding t as a variable, the system can be extended to a 3D system with (q, I, t) as the system space. We note that for a single branch, the system decays at a rate of $\sim \exp(-Rt/2L)$, which is obtainable by an analytical solution of periodic forced driving.

$$I = \dot{q} \tag{B6}$$

$$L\dot{I} = V_0 cos(\omega t) - q/C - f_{bi}(I) \tag{B7}$$

$$\dot{t} = 1 \tag{B8}$$

A 4-th order Runge-Kutta was used of a step size of $dt <$ 0.0000001s, which gives a sampling rate $\sim$ 10MHz, approximately $\sim$ 1000 times larger than the timescale of the fast dynamics. Decreasing the step size did not show any difference in the numerically solved solutions.

[1] Bocheng Bao, Q. Li, Ning Wang, and Xu Quan. Multistability in chua's circuit with two stable node-foci. *Chaos: An Interdisciplinary Journal of Nonlinear Science*, 26:043111, 04 2016.

[2] Rabinder N Madan. *Chua's Circuit: A Paradigm for Chaos*. WORLD SCIENTIFIC, 1993.

[3] Jean-Marc Ginoux and Christophe Letellier. Van der Pol and the history of relaxation oscillations: Toward the emergence of a concept. *Chaos: An Interdisciplinary Journal of Nonlinear Science*, 22(2):023120, 04 2012.

[4] A. S. Elwakil. Explaining hysteresis in electronic circuits. *International Journal of Electrical Engineering & Education*, 43(3):252–260, Jul 2006.

[5] Satyaki Kundu, Ranjan Kumar Patel, Srimanta Middey, and Bhavtosh Bansal. Dynamic hysteresis at a noisy saddle node shows power-law scaling but nonuniversal exponent. *Phys. Rev. E*, 108:024101, Aug 2023.

[6] Akira Utagawa, Tetsuya Asai, and Yoshihito Amemiya. Stochastic resonance in simple analog circuits with a single operational amplifier having a double-well potential. *Nonlinear Theory and Its Applications, IEICE*, 2:409–416, 10 2011.

[7] Myeong gi Jo, Subin Kim, Jeong Min Lee, and Eugene Park. Tunable negative differential resistor with an operational amplifier and n-channel mosfets. *Intermediate Physics Laboratory 2, Module 2*, Nov 2023.

[8] Hyungkwang Lim, Hyung-Woo Ahn, Vladimir Kornijcuk, Guhyun Kim, Jun Yeong Seok, Inho Kim, Cheol Seong Hwang, and Doo Seok Jeong. Relaxation oscillator-realized artificial electronic neurons, their responses, and noise. *Nanoscale*, 8:9629–9640, 2016.

[9] Petr Boriskov and Andrei Velichko. Switch elements with s-shaped current-voltage characteristic in models of neural oscillators. *Electronics*, 8(9), 2019.